Journal of Building Engineering 33 (2021) 101669

Contents lists available at ScienceDirect

Journal of Building Engineering

journal homepage: http://www.elsevier.com/locate/jobe

Durability characteristics of high and ultra-high performance concretes

Muazzam Ghous Sohail [a], Ramazan Kahraman [b,*], Nasser Al Nuaimi [a], Bora Gencturk [c], Wael Alnahhal [d]

[a] Center for Advanced Materials, Qatar University, P.O. Box 2713, Doha, Qatar
[b] Department of Chemical Engineering, College of Engineering, Qatar University, P.O. Box 2713, Doha, Qatar
[c] Sonny Astani Department of Civil and Environmental Engineering, University of Southern California, Los Angeles, CA, USA
[d] Department of Civil and Architectural Engineering, College of Engineering, Qatar University, P.O. Box 2713, Doha, Qatar

ARTICLE INFO

Keywords:
Concrete durability
High-performance concrete
Ultra-high performance concrete
Durability
Service life analysis

ABSTRACT

Durability characteristics of high-performance concrete (HPC) and ultra-high performance concrete (UHPC) are evaluated in comparison to normal strength concrete (NSC). HPC and UHPC are cast using commonly available materials with no special heat treatment. Concrete resistivity, rapid chloride permeability, sorptivity, porosity, and resistance to chloride migration and carbonation of these three types of concrete are assessed. Microstructure and hydration products are investigated using scanning electron microscope (SEM) imaging and X-ray diffraction (XRD) analyses, respectively. Potential enhancement in the service life of reinforced concrete (RC) structures when concrete is replaced with HPC and UHPC is predicted using the time-to-corrosion model. Dense microstructures, high electrical resistance, negligible chloride permeability, low sorptivity, no carbonation ingress are observed in HPC and UHPC. The chloride diffusion coefficient was found to be at least three orders of magnitude lower in UHPC compared to NSC, which could delay the corrosion initiation of steel reinforcement. With such positive attributes, these concretes are expected to find more widespread application in concrete structures in harsh-climatic conditions. This paper provides additional data and analysis that could accelerate the adoption of these materials in practice.

1. Introduction

The durability of normal strength concrete (NSC) under harsh climatic conditions has become a significant challenge worldwide. Chlorides and carbon dioxide (CO_2) ingress through the intrinsically porous microstructure of the NSC and initiate the corrosion of the steel reinforcement. Once initiated, the reinforcement corrosion reduces the service life of reinforced concrete (RC) structures. This issue is aggravated more so in the coastal and arid climatic regions [1,2]. Carbonation is reported to be more rapid in the industrial and coastal areas [1,3], where either higher CO_2 concentrations or the optimum conditions of humidity (40%–80%) and temperature (20-50°C), or both, are encountered. The CO_2 concentration in air is about 0.45%; however, in industrial zones and high traffic areas, CO_2 concentration may reach up 1% [4]. Sohail at al [1] reported concrete cover carbonation between 30 mm and 75 mm in RC structures after 30–50 years of exposure in Doha, Qatar. The carbonation rate was as high as 8 $mm/\sqrt{year}$. While, the chloride ion concentration at the steel-concrete interface was found to be 4 to 6 times higher than the threshold values for corrosion initiation for mild steel. The underlying reason for these observations was the inadequate quality of concrete to withstand the severity of the environmental conditions [1].

The quality of concrete is critical in weathering the harsh climates and preventing the corrosion of steel rebar; hence, rendering a resilient and durable civil infrastructure. High-performance concretes (HPC), and ultra-high performance concretes (UHPC), due to their dense microstructure are expected to address this durability issue in conventional RC structures. HPC can have a compressive strength of around 100 MPa and a workability equivalent to that of self-compacting concrete (SCC), which is typically between 455 mm and 810 mm as measured according to ASTM C143/C143M-15a [5]. UHPC, on the other hand, has a compressive strength that exceeds 150 MPa and has even higher flowability than SCC [6–9]. Such high strength and flowability are due to a high packing density and low porosity. These attributes are achieved by lowering the water-to-cement (w/c) ratio to between 0.2 and 0.3, adding a high amount of superplasticizers, and by using an optimum blend of

* Corresponding author.
E-mail address: ramazank@qu.edu.qa (R. Kahraman).

https://doi.org/10.1016/j.jobe.2020.101669
Received 2 April 2020; Received in revised form 21 May 2020; Accepted 13 July 2020
Available online 21 July 2020

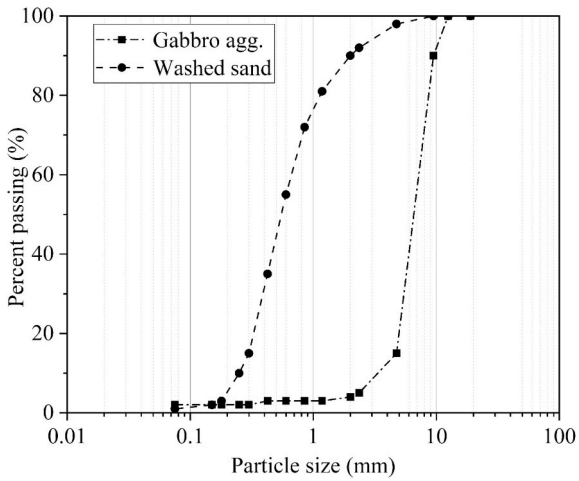

Fig. 1. Particle size distribution curves for coarse and fine aggregates.

supplementary cementitious materials (SCM) such as silica fume (SF), fly ash (FA), glass powder (GP) and rice husk ash (RHA) [1,10–12]. Commonly accepted non-proprietary UHPC mixture designs are still not available. A wide range of ingredients is used depending on the geographical location to design UHPC mixtures [10,13–16]. Proportioning of these ingredients is usually decided upon by combining information from particle size distribution (PSD) curves with analytical packing density models and trial-and-error. Rui Yu [17], Wang et al. [18], and Yu et al. [19] employed the modified Andersean and Andersen (modified A&A) curve, presented in Funk and Dinger [20], to achieve an optimum particle packing density of dry ingredients of UHPC. While de Larrard and Sedran [21] used analytical models to maximize the packing density of dry ingredients to achieve UHPC with strengths up to 200 MPa. Wong et al. [22] proposed a three-tier system for developing UHPC depending upon the optimum wet-packing-density of the cementitious materials. The optimum ratio of cement and SCMs for maximum flowability and strength is achieved at the first stage, then sand and the coarse aggregates are added successively in the cementitious matrix. The reason behind optimizing the wet-packing-density is to minimize the electrostatic and frictional forces between the fine particles in dry state [22,23]. It was reasoned that the maximum wet packing density of the matrix is what actually is required in the cementitious mix than the dry packing density.

Recently, more streamlined methods to design UHPC have been developed. Wille et al. [15] optimized the packing density of the UHPC mixture based on the maximum flow-spread criterion using a slump cone test and achieved UHPC with a compressive strength exceeding 150 MPa. Ingredients with varying grain sizes were employed and their effects on flow and strength were investigated. An optimum ratio of ordinary Portland cement (OPC): SF: GP equal to 1:25:25 was recommended. Two silica-sand sizes of 200 μm and 800 μm were employed in the UHPC matrix. Hence, a high percentage of fine particles were added to achieve a dense microstructure and a compressive strength above 150 MPa. Aghdasi et al. [24] used the same method to achieve a compressive strength of up to 168 MPa. To achieve a higher flowability of the mix, the cement and sand were replaced with a round-shaped FA at different proportions. It was observed that 30% replacement of sand with FA results in the highest flow and strength.

Regarding long-term durability, it has been established that UHPC could enhance the structural lifespan by slowing down the ingress of deleterious agents towards the steel-concrete interface [9,25]. Voort [26] reviewed the durability properties of UHPC. It was reported that UHPC has a chloride ion permeability and oxygen diffusivity that are 34 and 220, and 10 and 100 times less than HPC and NSC, respectively. However, the studies included in Voort [26] focused on reactive powder concrete (RPC), which is an earlier and uncommon type of UHPC fabricated via heat-curing at high temperatures [26–30]. Roux et al. [28] observed that in addition to a very low water absorption, the gas and chloride diffusion of RPC is two orders of magnitude lower than those of NSC. Tam et al. [27] found that the drying shrinkage of RPC is sensitive to w/c ratio and the amount of SP used. With a lower w/c ratio, a relatively low shrinkage and water absorption were observed, which were attributed to the dense microstructure and disconnected capillary pores. Graybeal and Tanesi [9] investigated the abrasion, scaling, freezing-and-thawing, and chloride resistance of UHPC treated under four types of curing regimes: i) steam curing at 90°C and 95% RH starting from 4 h of demolding, ii) untreated, iii) treated in tempered steam at 60°C initiating at the 15th day of casting (called as delayed curing). It was observed that the charge transferred in rapid chloride permeability test (RCPT) was 18 Coulombs, 360 Coulombs, 76 Coulombs, and 18 Coulombs for steam cured at 95°C, untreated, tempered cured, and delayed cured samples, respectively. These values are very low compared to what is observed in normal strength concrete [1,31,32]. While during abrasion testing, it was observed that the untreated samples lost one order of magnitude more mass than the steam cured ones.

UHPC employs a high amount of cement and SCMs, which may cause microcracks in the cementitious matrix due to early age plastic shrinkage. These cracks increase the chloride permeability and may initiate the corrosion of distributed steel fibers, especially in coastal zones. The cracking and corrosion of the steel fibers could reduce the tensile strength of the UHPC [33,34]. Yoo et al. [33] studied the effect of autogenous self-healing and fiber corrosion on the tensile properties of ultra-high performance fiber reinforced concrete (UHPFRC). It was reported that up to 3 μm cracks could be completely self-healed due to the hydration of unhydrated cement and the pozzolanic reaction of SCM. This self-healing increases the tensile performance of UHPFRC compared to the uncracked matrix. At the same time, it was observed that the corrosion of the surface of the steel fibers could enhance the tensile strength, strain-hardening in tension, and the fiber-matrix bond strength in UHPC. Yoo et al. [34] studied the effect of the degree of corrosion (2–8% by weight) of steel fibers and the effect of rust layer on the tensile properties of UHPFRC. It was found that 4–6% of corrosion enhances the tensile properties of UHPFRC compared to the case with no fiber corrosion. However, once the corrosion reaches 8%, the tensile strength, strain capacity, and energy absorption are reduced. Nevertheless, the tensile strength and energy absorption, even at 8% of corrosion by weight of steel, satisfied the minimum tensile strength requirement of 8 MPa and the minimum energy absorption requirement of 150 kJ/m^3, as specified in the Association Francaise Genie Civil (AFGC) recommendations [35]. Hashimoto et al. [36], after studying the effect of crack width opening on the tensile softening of UHPC reinforced with steel fibers, concluded that cracks up to 0.5 mm width, have no effect on the tensile strength or corrosion of steel fibers. It was reported that cracks larger than 0.5 mm could cause fiber corrosion, which in turn results in a higher tension softening behavior.

This study develops an HPC and a UHPC mixture using commonly available materials and no special heat treatment and investigates the durability characteristic of HPC and UHPC in comparison to NSC through accepted laboratory tests. Compressive strengths of 100 MPa and 150 MPa are, respectively, targeted in the material development of HPC and UHPC. The carbonation resistance of HPC and UHPC was tested under accelerated carbonation testing. Time-to-corrosion initiation was estimated using Fisk's second law of diffusion. Such concretes are becoming a necessity to arrest the rapid deterioration of RC structures, especially in harsh climatic regions. The data presented here is expected to shed light on the long-term durability of HPC and UHPC for more widespread implementation of these materials in practice.

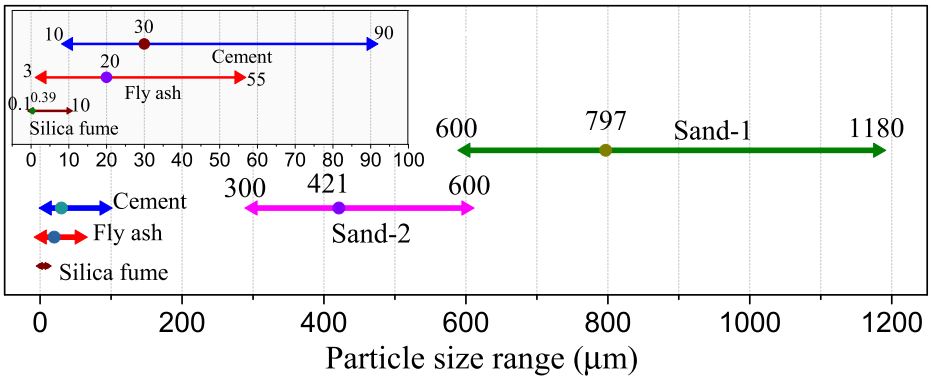

Fig. 2. Particle sizes of ingredients used in UHPC. Arrows represent the minimum and maximum, while the dot shows the median particle size.

Table 1
Oxides in OPC, SF, and FA obtained from XRF analysis.

Oxides[a]	Cement (OPC)	Silica Fume	Fly Ash	Sand-1	Sand-2
Na_2O (%)	–	0.04	0.06	–	–
MgO (%)	2	0.23	1.57	0.9	0.91
Al_2O_3 (%)	3.18	1.44	28.49	3.9	4.11
SiO_2 (%)	15.74	94.5	55.97	67.05	75.09
P_2O_5 (%)	–	0.53	0.62	1.3	0.93
SO_3 (%)	3.8	2.14	0.51	4.78	2.31
CL (%)	0.05	0.16	0.12	1.71	2.13
K_2O (%)	0.47	0.37	1	0.7	0.02
CaO (%)	68.91	0.16	2.74	17.44	12.71
TiO_2 (%)	0.28	–	1.95	0.23	0.16
V_2O_5 (%)	0.05	–	0.04	–	–
Cr_2O_3 (%)	0.05	–	0.04	0.12	0.13
MnO (%)	0.09	0.02	0.09	0.05	0.04
Fe_2O_3 (%)	4.8	0.42	6.63	1.7	1.35
NiO (%)	–	–	0.02	0.04	–
Rb_2O (%)	–	–	0	–	–
SrO (%)	0.05	–	0.06	0.08	0.05
Y_2O_3 (%)	–	–	0	–	–
ZrO_2 (%)	–	–	0.07	–	–
ZnO (%)	–	–	–	–	0.02
Ta_2O_5	–	–	–	–	0.03
Alkali (Na_2O + 0.658 K_2O) (%)[b]	0.68	1.07	3.27	–	–
Pozzolanic activity[b]	–	110	–	–	–
Los on ignition (%)[b]	1	2.1	1.2	–	–

[a] Equipment used does not detect lighter oxides, that is why % oxides are less than 100.
[b] Information provided by the supplier.

2. Materials and methods

2.1. Materials and preparation methods

2.1.1. Properties of material ingredients

OPC, complying with CEM I 42.5R [37] and provided by a local manufacturer, was used with target compressive strengths of 150 MPa, 100 MPa, and 40 MPa for UHPC, HPC, and NSC, respectively. Gabbro aggregates and washed sand constituted the coarse and fine aggregates, respectively, in NSC and HPC. Fig. 1 shows the PSD curves for the used coarse and fine aggregates. The maximum coarse aggregate size was limited to 10 mm to achieve homogenous and self-compacting mixtures for HPC and NSC. Epsilon PC 485 [38], a polycarboxylate ether-based admixture, was used as a high-range-water-reducer (HRWR) for all concretes.

UHPC mixture comprised of two fine sand sizes: sand-1 with a particle size range from 600 μm to 1.18 mm and sand-2 with a particle size range from 300 μm to 600 μm. These sands were obtained through a sieve analysis of one type of washed sand that was available locally for this study. Sand-1 and sand-2 made up to 65% of the total washed sand by weight. The remaining 35% of the sand contained either larger particles up to 4.75 mm or very fine sand below 300 μm, both of which are considered unfit for UHPC; and therefore, were discarded. Larger particles could inhibit a proper packing, while finer sizes increase the water demand; hence, reduce the flowability and strength. For the same reasons, coarse aggregates were omitted from the UHPC to increase the homogeneity and eliminate weak inclusions within the matrix. SF and FA were used both in HPC and UHPC. The particle size analysis of FA, OPC, sand-1, and sand-2 was carried out using a Malvern Master Sizer 3000®. While for SF, the Zetasizer Nano ZS (Malvern) equipment was used. The sonication of these finer particles (i.e., SF, FA, and OPC) was performed for 15 min before the analysis to avoid agglomeration, which results in erroneously identifying larger particle sizes. Fig. 2 shows the ranges of particle sizes used in UHPC. Arrows present the minimum and maximum sizes, while the dot shows the median size for each ingredient. The largest particle size of 1.18 mm (1180 μm) in UHPC was from sand-1, while the smallest was 0.1 μm from the SF. Median particle sizes of sand-1 and sand-2 were 797 μm and 421 μm, respectively. SF showed a particle size range between 0.1 μm and 10 μm, with a median particle size of 0.39 μm. The FA had a particle size range between 3 μm and 55 μm with a median of 20 μm. The particle size of OPC ranged between 10 μm and 90 μm with a median of 30 μm. The uniformly dispersed rounded fine particles of FA and SF render a denser and more homogeneous UHPC matrix.

UHPC has a very brittle matrix; and therefore, steel, synthetic, natural, or hybrid fibers are commonly used in UHPC. However, since the focus of this study is to evaluate the durability of the cementitious matrices, fibers are omitted from UHPC for a fair comparison with HPC and NSC. Fibers could also interfere with the applied currents and voltages during durability testing. In addition, it was reported that fibers have no impact on the particle packing density and play no role in the homogeneity of the matrix because their size is of the same order of magnitude of the large aggregates [39].

With regards to the chemical composition of these ingredients, Table 1 presents the major and minor oxide compositions of SF, FA, OPC, sand-1, and sand-2, obtained through X-ray fluorescence (XRF) analysis using a S2 Puma Bruker®. The amount of silica in SF was 94% with a pozzolanic index of 110 (as per the supplier). FA, sand-1, and sand-2 had silica contents of 56%, 67%, and 75%, respectively. Crystalline silica in sands create a bond between the sand particles and other products in the cementitious matrix during the hydration process. While the amorphous silica in SCM react with the calcium hydroxide ($Ca(OH)_2$) in the hydrated concrete matrix to form secondary calcium-silicate-hydrates (C–S–H) gel, which not only consumes portlandite but also increases the strength. As seen in Table 1, the silica contents of all ingredients were high.

Table 2
Mixture proportions of NSC, HPC, and UHPC.

Ingredients	NSC	HPC		UHPC	
	kg/m^3	kg/m^3	Ratio by % wt. of OPC	kg/m^3	Ratio by % wt. of OPC
OPC	400	645	1	820	1
Silica fume	–	128	0.2	190	0.23
Fly ash	–	128	0.2	150	0.18
Sand (max. particle size of 4 mm)	955	700	1.09	–	–
Sand-1	–	–	–	718	0.87
Sand-2	–	–	–	320	0.39
Coarse aggregates (max. particle size of 10 mm)	950	555	0.86	–	–
Water	159	200	0.31	173	0.21
HRWR	5	10	0.02	25	0.03

Table 3
Corrosion risk as a function of cementitious material resistivity [50].

Resistivity (Ohm-cm)	Corrosion risk
>20,000	Negligible
10,000 to 20,000	Low
5,000 to 10,000	High
<5,000	Very High

2.1.2. Proportioning of UHPC

A reproducible UHPC mixture with optimum wet-packing density, flowability, and maximum possible strength without using any specialized mixing or heat treatment technique, was achieved through experimental iterations. To achieve a target compressive strength of 150 MPa with high flowability, a range of quantities of OPC, SCMs, sand, water, and HRWR was established through an extensive literature review on UHPC from the 1990s until 2016, as presented in Sohail et al. [6]. Those ingredients which are readily available in the local construction market and have been employed by several other researchers [13,14,31], were selected. A similar concept to that presented in Wille et al. [15] and Wong and Kwan [22], which involves optimizing the maximum wet-packing-density of ingredients for maximum flow and strength, was employed. However, instead of obtaining the optimum flow and strength of cementitious materials separately, the sands were added in the mix at the start. The flow of the mix was recorded according to ASTM C1437-15 [40], and the compressive strengths of 50 × 50 × 50 mm cubes were measured at 7 days and 28 days of curing. The quantity of each ingredient was changed, and its effects on flow and strength were determined until the desired strength with acceptable flowability was achieved. Around 40 trial mixes were carried out to obtain the optimal results. Initially, an OPC: SF: FA ratio of 1:0.25:0.25 was employed, which was based on the recommendations by Wille et al. [15]. In this study, FA was employed instead of GP, also sands were added with other cementitious materials in the dry state. Therefore, the highest strength and flow were achieved with an OPC: SF: FA ratio of 1:0.23:0.18. The total sand ratio by weight of OPC was 1.25, of which sand-1 was equal to 0.88 and sand-2 was equal to 0.37. The w/c ratio was 0.23, and the water-to-binder (w/b) ratio was 0.178. The HRWR amount was 3% by wt. % of OPC. Table 2 presents the mixture proportions for NSC, HPC, and UHPC.

Mixture proportioning information is readily available for HPC and NSC. For HPC, the design procedure presented in Ref. [41] was used. However, the procedure in Ref. [41] is for a material with 55–70 MPa compressive strength, while, in this study, an HPC with 100 MPa strength is desired. Adjustments to OPC, SF, FA, sand, aggregate quantities, and w/c ratio were made to achieve the desired 100 MPa strength. The NSC mixture was based on readily employed designs for structural concrete.

2.1.3. Mixing procedure

The mixing procedure and the type of mixer used are as crucial as the material selection in obtaining the desired properties of UHPC. The liquefaction time, workability, and strength of the UHPC, all depend on the preparation method [12,42]. Since very fine ingredients are employed in UHPC, to overcome the electrostatic and friction forces that cause agglomeration, a higher amount of energy is required during mixing. Hence, an intensive mixer is needed. It is necessary to achieve a homogeneous dry-mix before adding liquid ingredients to avoid the agglomeration of the fine particles. It has been observed that the stepwise addition of liquid HRWR enhances the dispersion of these fine particles and increases the flowability [43,44].

A 5 L pan mixer was used for the trials of UHPC, while a 95 liters pan mixer was used to produce larger quantities during casting of cylindrical (100 × 200 mm) and prismatic (100 × 100 × 350 mm) samples. In both cases, ingredients were first dry-mixed for 5 min, then half of HRWR was slowly poured into the mix of dry materials in 1 min, and mixing was continued for 2 more minutes. The remaining half of the HRWR was mixed with water and poured in the mix slowly over a 1 min period. As mentioned earlier, because of the very low w/c ratio of UHPC, it demands a higher amount of energy during the mixing of the dry ingredients. For this reason, the time it takes for a mixture to become a flowable paste became an essential parameter. Hence, the time required for a mixture to turn into a flowable paste after adding all the liquid ingredients has become known as the liquefaction time [24].

Although the liquefaction time depends on the relative amounts of HRWR, FA, OPC, and SF, it was found that the most influential ingredient is the FA, a higher amount of which reduces the liquefaction time. Other factors such as the dryness of the mixer walls, slight variations in the speed of addition of the water and the HRWR, and the temperature and humidity of the mixing environment were also found to affect the liquefaction time. The liquefaction time of the optimized mixes was between 2 min and 4 min in both 5 L pan mixer and 95 L pan mixer. The mixing of NSC and HPC were carried out in a conventional gravity mixer.

2.2. Fresh and hardened properties

The flowability of UHPC was measured according to ASTM C1437-15 [40] while the flow spread of NSC and HPC were measured according to ASTM C1611/C1611M-14 [45]. The compressive strength of NSC, HPC, and UHPC was measured on 100 × 200 mm cylinders according to ASTM C39/C39M-17 [46] at 28 days of curing, while the flexural strength was measured on 100 × 100 × 350 mm prisms at 28 days of curing according to ASTM C78/C78M-15a [47].

2.3. Durability characterization methods

The quality of the cementitious materials was assessed based on resistivity, porosity, sorptivity, and resistance to chloride migration and CO_2 penetration measurements. These parameters are considered good indicators of whether a cementitious material will withstand the harsh environmental conditions in service. The details of the tests performed are described in the following.

2.3.1. Resistivity

The resistivity of a cementitious material indicates whether the reinforcing steel is susceptible to corrosion or not [48,49]. A lower resistivity is associated with a higher risk of corrosion and vice versa. Alongside several other factors that affect the resistivity, the microstructure formation is the most important. A dense cementitious matrix shows a higher electrical resistivity. In this study, the resistivity was measured using a four-point Wenner probe from Giatec®, in accordance with AASHTO TP 95 [50]. Measurements were performed on three cylindrical samples of 100 × 200 mm dimensions from each material at 28 days of curing. The degree of saturation of concrete and type of pore

solution affect its resistance to the electrical charge. The electrical resistance of concrete varies from 50 Ohm-m in saturated state to 10^9 Ohm-m in a completely dry state [51]. Thus, it is recommended to test concrete samples in a saturated surface dry (SSD) condition to obtain reliable and repeatable results for comparison purposes [52]. For these reasons, the samples in this study were tested in a quasi-saturated state just after the 28 days of curing. Table 3 presents the corrosion risk associated with different ranges of concrete resistivities. When the resistivity is higher than 20,000 Ohm-cm, the corrosion risk is negligible, while for resistivity less than 5,000 Ohm-cm, a very high risk of corrosion exists.

2.3.2. Chloride permeability

The ability of chloride ions to penetrate through concrete was determined using the rapid chloride permeability test (RCPT) in accordance with ASTM C1202-12 [53]. The experiments were carried out on disk samples of 100 × 50 mm dimensions sliced from 100 × 200 mm concrete cylinders after 28 days of curing. The disks were dried in an oven at 50°C for three days, and then silicone epoxy was applied on the cylindrical surface of the samples. The samples were then placed inside a desiccator under 50 mbar vacuum environment for 3 h. After 3 h of vacuuming, water was poured in the desiccator through a valve such that the samples are completely immersed. The vacuuming was continued for another 18 h. After the conditioning, the samples were mounted between two polycarbonate boxes, out of which, one was filled with 0.3 N NaOH solution and the other one with a 3% by weight sodium chloride (NaCl) solution. A 60 V potential was applied between the terminals of the two containers. Due to the applied voltage, the current flows through the concrete disk samples. The total charge transferred, Q, is calculated (in Coulombs) according to

$$Q = 900(I_0 + 2I_{30} + 2I_{60} + \cdots + 2I_{300} + 2I_{330} + I_{360}) \quad (1)$$

where I_0 is the current (in Amperes) immediately after the voltage is applied, and I_{30}, $I_{60,}$ and so forth, are the currents after every 30 min. The resistance to the chloride ingress and the predicted quality of the cementitious materials are associated with the amount of charge transfer [53].

2.3.3. Porosity

The porosity of the cementitious matrix greatly influences the durability of RC structures. Harmful agents penetrate easily through the concrete cover if the pores have a high volume, large diameter, and if they are interconnected. The porosity of NSC, HPC, and UHPC was measured according to ASTM C1754/C1754M-12 [54]. Cylindrical concrete samples of 100 × 200 mm were sawed into 100 × 50 mm sized disk specimens. The obtained specimens were dried at 38 °C, and the weight was monitored every 24 h until the change is less than 0.5%. Then samples were immersed into water for 30 min, and the submerged weight was recorded. The total void contents were calculated based on the sample dimension, the dry weight, and the submerged weight through a relation provided by ASTM C1754/C1754M-12 [54].

2.3.4. Sorptivity

Sorptivity is another important parameter for the durability assessment of cementitious materials, and it indicates how easily moisture containing deleterious agents can ingress through the concrete cover. It also indicates the capacity of cementitious material to absorb water through the capillary pores. Sorptivity was measured in accordance with ASTM C 1585-13 [55] on disk samples of 100 × 50 mm dimensions sliced from concrete cylinders of 100 × 200 mm dimensions at the age of 28 days. Three specimens cut from the middle of the cylinders were tested for each material. Samples were conditioned in an environmental chamber at 50°C and 80% RH for 3 days and then stored in a laboratory environment at 23°C for 15 days to stabilize the moisture content in the capillary pores. Then, the cylindrical surfaces of these disk samples were covered with silicone epoxy. Samples were dipped into distilled water inside a large container in such a way that the whole cross-sectional area is exposed to water, and the samples were immersed up to only 1 cm depth underwater. Weight measurements were recorded at intervals recommended by ASTM C 1585-13 [55]. The absorption, I, is calculated according

$$I = \frac{m_t}{a^* d} \quad (2)$$

where m_t is the change in mass (g) at time t (sec), a is the exposed area (mm^2) to water, and d is the density of the water in g/mm^3. Absorption is plotted against the square root of time, t, to obtain the absorption rate, which is the sorptivity in $mm/\sqrt{sec}$. The first 6 h of readings provide the initial sorptivity, while readings from 24 h to 7 days provide the secondary sorptivity. The initial sorptivity indicates the ability of concrete to absorb water from the atmosphere in a dry state. The secondary sorptivity indicates a saturated state of concrete pores. The rate of absorption at the early age of contact with moisture determines how easily water would penetrate and then evaporate. This process facilitates the concentration of salts that the evaporating water will leave inside the concrete pores. In this study, only the initial sorptivity is reported since the secondary sorptivity may not be possible in UHPC due to very slow initial sorptivity in the very low porosity matrix.

2.3.5. Chloride diffusivity

Corrosion of reinforcement initiates when a certain chloride concentration is achieved at the steel-cementitious material interface. Models predicting the time-to-corrosion are based on the diffusion properties of the cementitious material. HPC and UHPC are expected to have a very low chloride diffusivity due to the disconnected capillary pores and the dense microstructure. The chloride diffusion coefficient was determined in accordance with ASTM C1556-11a [56]. Cylindrical specimens of 100 × 200 mm were saw cut to disk samples of 100 × 70 mm dimensions. Silicone epoxy was applied to the cylindrical surfaces of the samples. Then, the samples were immersed in a saturated calcium hydroxide solution for three days or until the weight change becomes constant. Then samples were rinsed with tap water and immersed in a 3.5% by weigth NaCl solution. The ASTM standard specifies a minimum immersion of 35 days; however, since a low w/c ratio was used in HPC and UHPC, to allow chloride to penetrate in these materials, the samples were kept under the solution for 95 days. The initial chloride contents were measured by cutting a 100 × 20 mm disk from the parent cylinder. This was to account for the chlorides introduced by its ingredients or by accidental exposure to the saline environment before testing. After conditioning, 4 mm thick slices were cut from each sample and ground to an average 125 μm particle size. The chloride content in the powders was determined in accordance with BS 1881:Part-124 [57].

The chloride diffusion coefficient was estimated by measuring the chloride contents at different depths. This chloride profile along the depth was fitted to the following nonlinear regression

$$C(x,t) = C_s - (C_s - C_i).\mathrm{erf}\left(\frac{x}{\sqrt{4.D_a.t}}\right) \quad (3)$$

where $C(x,t)$ is the chloride content (in % mass) at a depth x and exposure time t (sec), C_s is the projected chloride contents in % mass at the interface, which is exposed to the liquid, C_i is the chloride contents in % mass prior to immersion in the NaCl solution, and D_a is the apparent diffusion coefficient in m^2/s.

2.3.6. Carbonation

The carbonation of concrete cover is another major factor that may initiate the corrosion of reinforcing steel bars by reducing the pH of the cementitious matrix. In this study, NSC, HPC, and UHPC cylinders were placed in an environmental chamber at 50% CO_2, 60% RH, and 23°C at 28 days of curing to study the carbonation rate. The concentration of

Table 4
Fresh and hardened properties of tested cementitious materials.

Properties	NSC	HPC	UHPC
Flow (mm)	535[a]	586[a]	280[b]
T_{50} (s)	8	6	NA
28 days compressive strength (MPa)	38	93	161
28 days flexural strength (MPa)	4	7	11

[a] According to ASTM C1611-14 [45].
[b] According to ASTM C1437-15 [40].

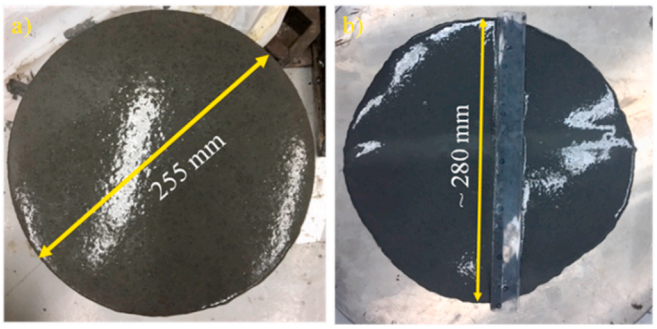

Fig. 3. Cone flow test of UHPC: a) flow spread on the recommended table, b) flow spread on a flat steel plate.

CO_2 was at least 100 times higher than a natural environment to accelerate the carbonation process. The carbonation depth was measured using phenolphthalein spray on the sawed surfaces after 3 months and 6 months of exposure. The carbonation rate is calculated according to

$$x = A\sqrt{t} \tag{4}$$

where x is the depth of carbonation in mm after time t *(year)*, while the A is the rate of carbonation in mm/$\sqrt{\text{year}}$.

2.4. Microstructural imaging and mineralogical analysis

The microstructure formation was studied using scanning electron microscopy (SEM) imaging of the broken cementitious material surfaces at different magnifications using a FE SEM NOVA® instrument. The mineralogy of the hydrated cementitious matrices was obtained using an X-ray diffraction (XRD) analysis carried out using a PAN analytical® EMPYREAN with $C_u - K_\alpha$ radiations. The scan was run at 2Θ values from 10° to 90°, and the step size was 0.01°. These tests were performed after 90 days of casting to ensure that the hydration process is complete.

2.5. Service life Evaluation

The degradation in RC structures can be divided into two distinct time phases: initiation, and propagation as in

$$T = T_i + T_{cr} \tag{5}$$

where T_i is the initial phase until the initiation of corrosion and T_{cr} is the time after corrosion initiation. The initial phase depends on the quality of the cementitious material, its diffusion coefficient, porosity, absorption, and the cover thickness used. This phase lasts until a sufficient amount of chloride ions diffuse through the cover and accumulate at the steel-concrete interface to initiate the corrosion of the steel reinforcement. While the propagation phase, T_{cr}, is the time from corrosion initiation until enough corrosion-products are formed at the steel-concrete interface to distress the concrete and cause cracking and spalling. The concrete cracking is either considered as the end of service life or time-to-repair. However, T_{cr} is a short period of time and difficult to model due to several complex phenomena involved. For this reason, the corrosion initiation is considered by several researchers as the end of life of an RC structure.

In this study, the time-to-corrosion was calculated for NSC, HPC, and UHPC using

$$T_i = \frac{C_c^2}{4D_c\left(erf^{-1}\left(1-\frac{C_r}{C_s}\right)\right)^2} \tag{6}$$

where C_r is the chloride threshold of rebar in % wt. or kg/m^3, C_s is the surface chloride concentration in % wt. or kg/m^3, D_c is the diffusion coefficient in mm^2/year or m^2/sec, C is the cover thickness in mm, and $erf()$ is the statistical error function. The cover thickness was increased from 30 mm with 5 mm increments up to 75 mm.

3. Results and discussion

3.1. Fresh and hardened properties

Table 4 presents the fresh and hardened properties of the studied cementitious materials. The NSC and HPC had flow spreads of 535 mm and 586 mm, respectively, while T_{50}, i.e., the time to reach 50 cm spread, was 8 s and 6 s, respectively. The flow of the optimized UHPC mixture was 280 mm. Fig. 3 shows the spread diameter of UHPC in the cone test, according to ASTM C1437-15 [40]. The recommended cone in the standard was placed on a flat steel plate since the dimensions of the recommended brass table was not sufficient enough to cover the flow of UHPC (see Fig. 3).

Fig. 4 presents the cross-sectional views of 100 × 200 mm hardened cylinders of NSC, HPC, and UHPC. The texture of the cementitious materials gets finer from NSC to UHPC. NSC uses a high amount of coarse aggregates as compare to HPC, while coarse aggregates are omitted from UHPC in order to eliminate these weak inclusions. It is noteworthy to mention that some researchers have developed UHPC with coarse aggregates of up to 20 mm size [18].

The average compressive strengths of NSC, HPC, and UHPC measured on six cylinders at 28 days of curing were obtained as 38 MPa, 93 MPa, and 161 MPa, respectively. The failure modes of HPC and UHPC were distinctly different from NSC. NSC cylinders failed in the cement matrix, having failure lines passing through the length of the cylindrical test samples. While in the case of HPC and UHPC, the failures were through the aggregates and sand particles, demonstrating the higher strength of the cementitious matrix compared to the coarse and fine aggregates used. Due to the very high elastic energy stored close to maximum load and since no fibers were used, the UHPC samples failed with a sudden blast. The failure shape was conical in both the HPC and UHPC. The average flexural strength measured on three samples of each material was 4 MPa, 7 MPa, and 11 MPa for NSC, HPC, and UHPC, respectively. It is important to note that the bending test is normally performed on UHPC mixes with embedded distributed fibers, which drastically increase the flexural strength. Therefore, the results presented here should be interpreted as a representation of the UHPC cementitious matrix, not the UHPC material. The compressive and flexural strengths of NSC, HPC and UHPC are provided in Table 4.

3.2. Durability characteristics

Fig. 5 presents electrical resistivity values after 28 days of curing. Average values over three samples were obtained as 25 kΩ cm, 343 kΩ cm, and 480 kΩ cm, for NSC, HPC, and UHPC, respectively. HPC and UHPC had 13 and 18 times higher electrical resistivity than the NSC, respectively. These resistivity values are very high, according to AASHTO TP 95 [50], and no-corrosion risk is associated with such values. Electrical current passes through concrete pore solution, and if pores are interconnected and filled with ion carrying liquids, a lower

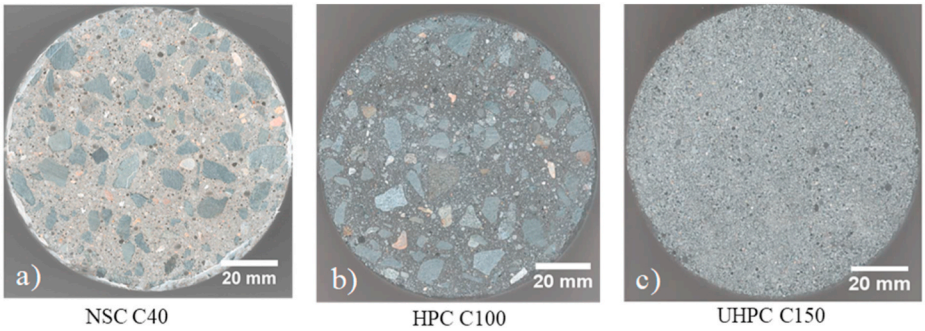

Fig. 4. Cross-sectional views of a) NSC, b) HPC, and c) UHPC concrete cylindrical samples.

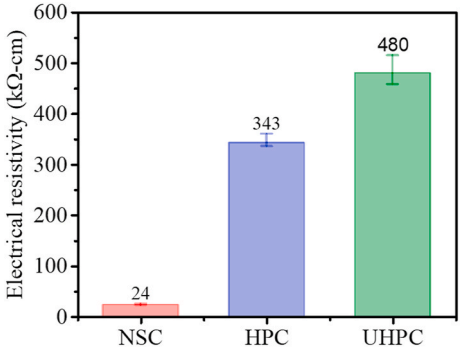

Fig. 5. Resistivity measured at 28 days according to AASHTO TP 95 [50].

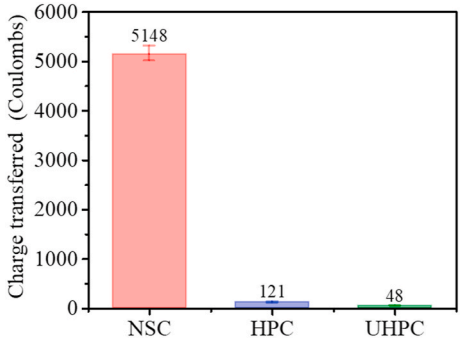

Fig. 6. RCPT charge transfer in NSC, HPC, and UHPC.

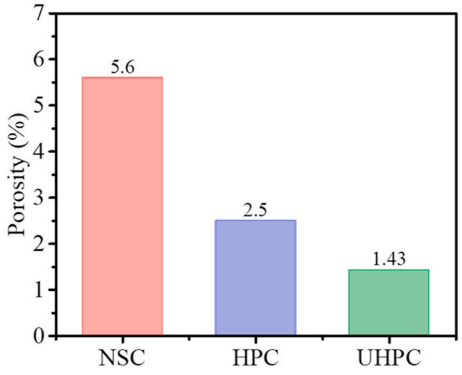

Fig. 7. Total measured porosity of NSC, HPC, and UHPC.

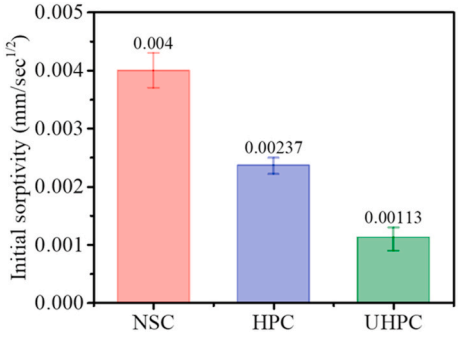

Fig. 8. Initial sorptivity values for NSC, HPC, and UHPC.

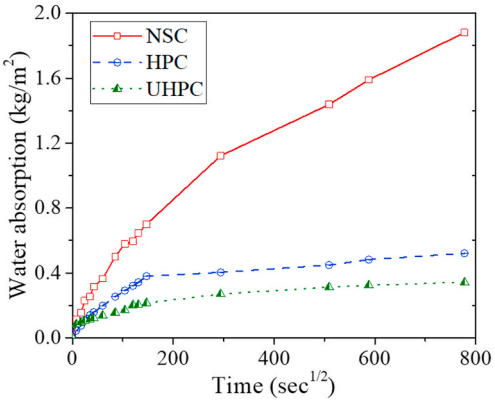

Fig. 9. Sorpitivity of NSC, HPC, and UHPC.

electrical resistivity is obtained. In the case of UHPC, the higher resistance to electrical current suggests that there is a lower number of smaller pores that are not interconnected. During the corrosion propagation phase, the higher concrete resistivity hinders the corrosion process at the steel-concrete interface by reducing the mobility of Fe^{2+} and OH^- ions. This reduces the formation of expansive rust products that distress the surrounding cementitious material. Hence, the cracking and spalling could be minimized with HPC and UHPC.

Fig. 6 presents a comparison of the RCPT values. Average values over three samples were 5,148 Coulombs, 120 Coulombs, and 48 Coulombs for NSC, HPC, and UHPC, respectively. The dense microstructure and discontinuous capillary pores of UHPC resist the flow of ionic charge while porous NSC permits these ions to pass relatively easily. Similar RPCT values were obtained for UHPC (i.e., less than 40 Coulombs) by Graybeal and Tanesi [9]. The chloride diffusion coefficient of concrete could also be estimated from the RCPT values [58]. The higher the charge transfer through the cementitious matrix is, the higher is the diffusion coefficient.

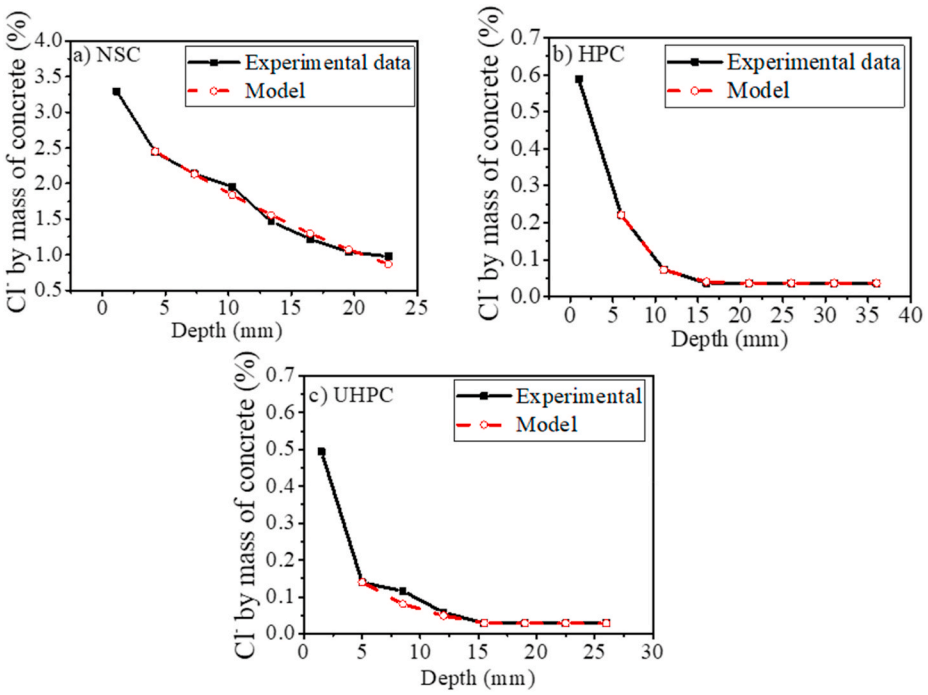

Fig. 10. Chloride profiles and curve fitting to calculate the diffusion coefficients: a) NSC, b) HPC, and c) UHPC.

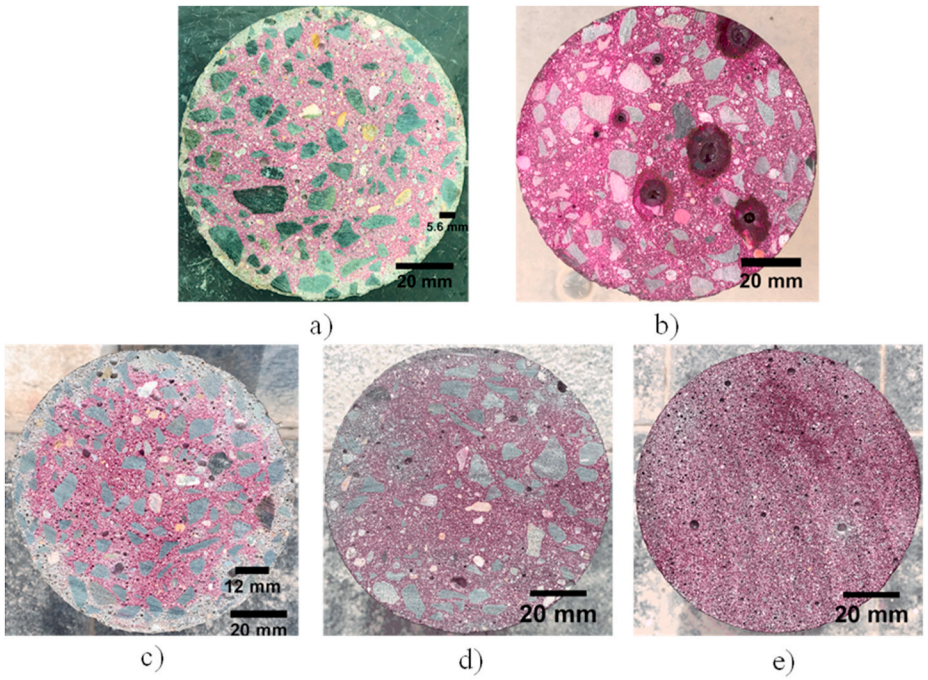

Fig. 11. Carbonation depths by phenolphthalein indicator: a) NSC and b) HPC after 3 months; c) NSC and d) HPC after 6 months, and e) UHPC after 6 months.

Fig. 7 shows the average porosity measured from three samples of NSC, HPC, and UHPC. UHPC had a porosity of 1.43%, while HPC and NSC showed a porosity of 2.5% and 5.6%, respectively. The lower w/c ratio, the presence of fine SCM, and the use of fine sand reduce the formation of larger pores and reduce the total porosity of the cementitious matrix. Such low porosity of UHPC slows down the ingress of water and other deleterious agents. Roux et al. [28] found the total porosity (defined as the space not occupied by the hydration products) of RPC to be around 1% with pore sizes ranging between 6 nm and 100 μm. Vernet 2004 [59] also suggested that the total porosity is not more than 1–2% in the case of UHPC. It was also suggested that the pore size range between 2 nm and 10 nm. Abbas et al. [60], through a literature review, also presented a similar range of values found by different researchers. These results confirm the findings of this study.

Fig. 8 presents the average initial sorptivity values of the studied cementitious materials. Average values as measured on three samples of each material were $40 \times 10^{-4}\ mm/\sqrt{sec}$, $23 \times 10^{-4}\ mm/\sqrt{sec}$ and $11 \times 10^{-4}\ mm/\sqrt{sec}$ for NSC, HPC and UHPC, respectively. The sorptivity of HPC and UHPC was significantly lower compared to NSC. During the immersion underwater, the intake curve shows a point of inflection,

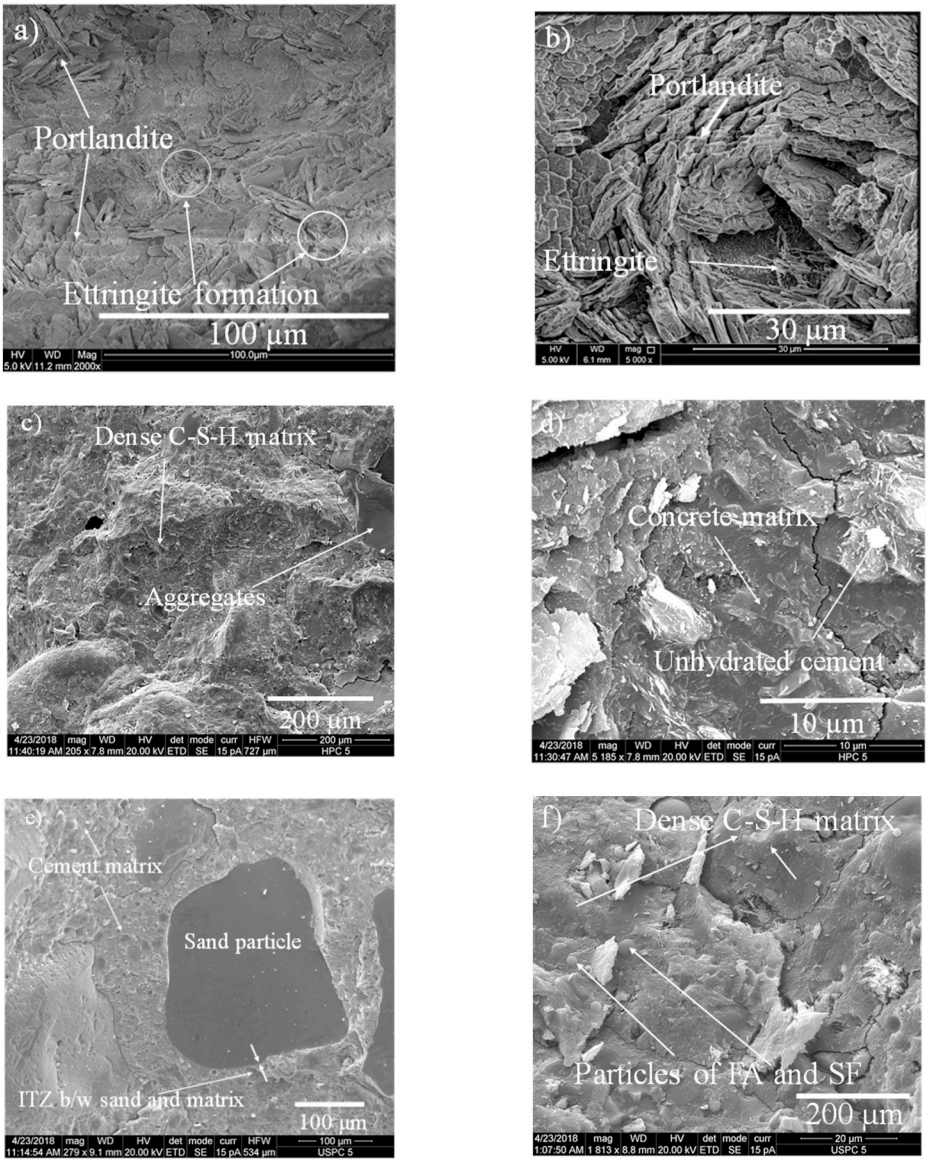

Fig. 12. Microstructural images of studied concretes: a, b) NSC, c, d) HPC, and e, f) UHPC.

indicating a shift from a transient to a steady-state absorption. To observe these inflection points, the curves were plotted from the first until the last reading point, as shown in Fig. 9. The point of inflection is seen in NSC and HPC. However, it was not obviously present in the case of UHPC, indicating that either capillary pores are missing in the UHPC matrix or the pore network is disconnected. Roux et al. [28] also observed a very low water absorption and no point of inflection in RPC and attributed it to disconnected capillary pores.

Lower water sorptivity of the cementitious material from the moist-air or seawater minimizes the ingress of deleterious materials such as Cl^{-} and sulfates. In addition, water is required for the carbonation process. Hence, with negligible water sorptivity, the carbonation process will be slowed down. With a low water sorptivity, the durability of RC structures could be enhanced in industrial and coastal areas where the carbonation is prevalent. With lower water entrapped in the concrete volume, the freezing and thawing effects could also be minimized in cold climatic conditions.

Fig. 10 presents the chloride concentrations at different depths after 95 days of exposure to a 3.5% by weight NaCl solution. Three samples for each concrete type were tested, readings for each depth were found to be similar over all samples. The chloride diffusion coefficients and estimation of surface chloride contents were done by fitting the profiles to Eq. (3) in accordance with ASTM C1556-11a [56]. As per the standard, the reading at the first depth that is at the surface was excluded during fitting. The diffusion coefficients were obtained as $1.32X10^{-11}\ m^2/sec$, $7.5X10^{-13} m^2/sec$ and $1.42X10^{-14}\ m^2/sec$ for NSC, HPC, and UHPC, respectively. UHPC had about three orders of magnitude lower chloride diffusion coefficient than NSC. This means to achieve the same chloride threshold at the steel-concrete interface by diffusion, a 1,000 times longer time period will be required; hence, time-to-corrosion initiation will be prolonged. Piérard et al. [61] observed an apparent chloride diffusion coefficient of $20 \times 10^{-14}\ m^2/sec$ in UHPC with a compressive strength from 140 MPa to 160 MPa. Vernet 2004 [59] suggests that the diffusion coefficient of UHPC is two orders of magnitude lower than that of HPC and three orders of magnitude lower than that of NSC. Roux et al. [28] estimated the diffusion coefficient for RPC by a method similar to RCPT, and the results were in the same range as those for UHPC in this study.

Fig. 11 shows the carbonation depth after conditioning the samples in the carbonation chamber for 3 months and 6 months. After three months in a 50% CO_2 environment, the carbonation front reached 5.6 mm in the NSC cylinders while it reached up to 12 mm after 6 months.

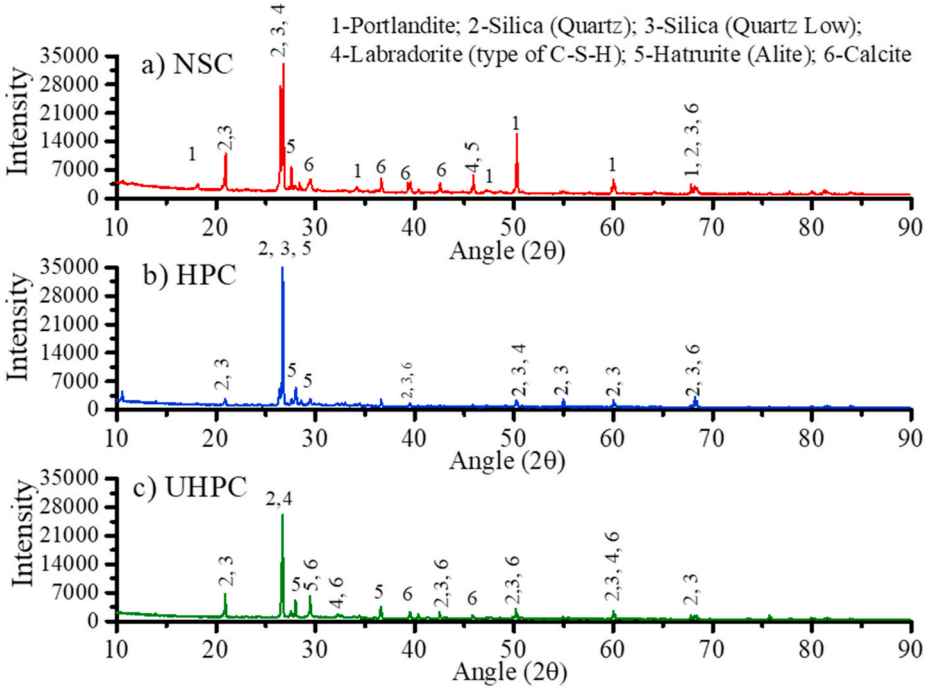

Fig. 13. XRD peaks of a) NSC, b) HPC, and c) UHPC.

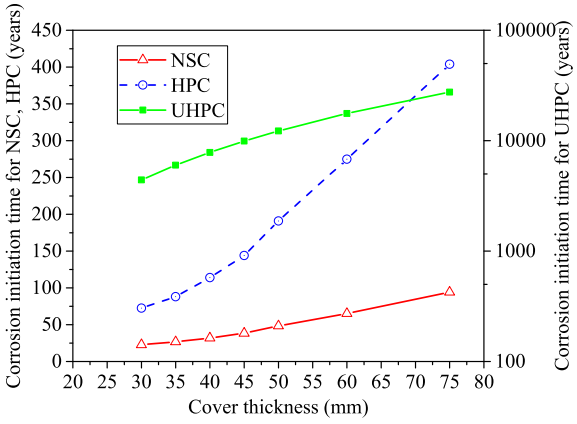

Fig. 14. Time to corrosion initiation from NSC and HPC for different cover depths.

This gives a carbonation rate, A, of 12–16 $mm/\sqrt{year}$ according to Eq. (4). On the other hand, there were no signs of carbonation in HPC and UHPC after 6 months in a similar environment. Similar observations are reported by Roux et al. [28] after placing RPC in 100% CO_2 environment for 42 days while a carbonation rate of 50 $mm/\sqrt{year}$ was observed in NSC samples with 30 MPa strength. The carbonation rate depends on the quantity of $Ca(OH)_2$ in the matrix, the concentration of CO_2, and the availability of H_2O. In the case of NSC, the $Ca(OH)_2$ constitutes up to 20% of the total hydration products, which increases the carbonation rate of concrete. In the case of HPC and UHPC, the composition of the hydrated matrix is different than that of NSC. The pozzolanic reaction in which the SCM react with $Ca(OH)_2$ to form C–S–H gel consumes the Ca $(OH)_2$ needed for the carbonation reactions.

3.3. Microstructural imaging

The SEM images of NSC showed the needle-like formation of ettringite and a large amount of $Ca(OH)_2$ crystals (see Fig. 12a and b). Heterogeneous formations were observed on the concrete surface. On the other hand, HPC and UHPC exhibited a very dense microstructure and a homogenous texture, as shown in Fig. 12c and d and Fig. 12e and f, respectively. Dense C–S–H gel is the major component of the cementitious matrix. Ettringite formation and crystalline structure of the Ca $(OH)_2$ are not observed. As explained above, the pozzolanic reaction converts the $Ca(OH)_2$ to C–S–H gel, which further enhances the strength and reduces the porosity. Lower w/c ratio also contributes to reduced Ca $(OH)_2$ formation during the hydration process. Fig. 12e shows that in the UHPC matrix, the interfacial transition zone (ITZ) between the cementitious matrix and the sand particles has a negligible thickness. The defect-free microstructure of UHPC ensures a resistance to chemical attack and the ingress of deleterious agents. Lower porosity, sorptivity, and higher electrical resistance exhibited by HPC and UHPC are due to this dense microstructure.

Fig. 13 presents the XRD peaks of NSC, HPC, and UHPC materials. The peaks of portlandite were only available in NSC, while in HPC and UHPC, these peaks were either not present or had very low intensities. The peaks of labradorite and hatrurite (alite) were prominent in the case of HPC and UHPC, indicating the presence of different phases of C–S–H formed due to the initial hydration of cement and by the pozzolanic reaction of the SCM.

3.4. Service life evaluation

The generally accepted chloride threshold value for mild steel is 0.4% by weight of cement [62,63]. This value was converted to % wt. of cementitious materials. For NSC, HPC, and UHPC, the chloride threshold was obtained as 0.06%, 0.09%, and 1.2% wt., respectively, while C_s was set to 0.05%. Fig. 14 shows the time-to-corrosion for NSC, HPC, and UHPC for different cover thicknesses. The initiation times for UHPC are presented on a logarithmic scale on the right of Fig. 14. It is observed that the time to corrosion increases by several folds if HPC and UHPC are employed. With 30 mm cover depth, the HPC had three times higher time-to-corrosion than NSC. While for UHPC with a 30 mm cover thickness and measured diffusion coefficient, the initiation time was 1950 years. Because of the delayed corrosion initiation and slow corrosion activity due to higher electrical resistivity, the repair cost

during the lifespan of a RC structure could be reduced or completed eliminated for HPC and UHPC.

It is to be noted here that these conclusions are based on un-cracked HPC and UHPC. As these concretes are very brittle in nature, cracking is expected and should be controlled using an appropriate amount of micro and macro fibers.

4. Conclusions

This study showed that HPC and UHPC could be a feasible and practical solution for the durability issues encountered in harsh climatic regions. These cementitious materials could be manufactured using commonly available ingredients and conventional mixing and curing methods to achieve compressive strengths of 160 MPa. A study on the durability characteristics of these materials yielded the following main conclusions.

- The HPC and UHPC have a very high electrical resistivity, i.e., 343 kOhm.cm and 480 kOhm.cm, respectively, which means that a very low corrosion risk is involved for steel rebar placed in these materials.
- The sorptivity of HPC and UPHC was between one-half and one-third of that of NSC. This could help reduce the absorption of water, which transports the chlorides and other harmful agents.
- The charge transfer in RCPT was as low as 48 Coulombs for UHPC, and 129 Coulombs for HPC. This shows the dense microstructure with less interconnected pores.
- The porosity of NSC, HPC, and UHPC was 5.5%, 2.65%, and 1.43%, respectively.
- Microstructural analysis of HPC and UHPC revealed a dense formation of C–S–H gel and smaller ITZ. Peaks of Portlandite were not present in XRD of NSC, while UHPC and HPC showed the presence of different phases of C–S–H gel as a result of the consumption of portlandite in the presence of SCM. These are the results of the pozzolanic reactions of FA and SF with portlandite.
- It was concluded that for UHPC there was no carbonation penetration after 6 months of exposure to a 50% CO_2 environment.
- The respective chloride diffusion coefficients in the case of HPC and UHPC were one and three orders of magnitude lower than that of NSC.
- The time to corrosion initiation with 30 mm concrete cover thickness was three and 78 times that of NSC for HPC and UHPC, respectively.

CRediT authorship contribution statement

Muazzam Ghous Sohail: Methodology, Investigation, Data curation, Formal analysis, Visualization, Writing - original draft, Writing - review & editing. **Ramazan Kahraman:** Resources, Funding acquisition, Supervision, Project administration, Investigation, Writing - original draft, Writing - review & editing. **Nasser Al Nuaimi:** Methodology, Resources, Funding acquisition, Supervision, Writing - review & editing. **Bora Gencturk:** Conceptualization, Methodology, Data curation, Resources, Funding acquisition, Investigation, Writing - original draft, Writing - review & editing. **Wael Alnahhal:** Resources, Investigation, Data curation, Formal analysis, Writing - original draft.

Declaration of competing interest

The authors declare that they have no known competing financial interests or personal relationships that could have appeared to influence the work reported in this paper.

Acknowledgements

The funding for this research was provided by the National Priorities Research Program of the Qatar National Research Fund (a member of the Qatar Foundation) under the award no. NPRP 7-410-2-169. The statements made herein are solely the responsibility of the authors and do not necessarily reflect the opinions of the Sponsor.

References

[1] M.G. Sohail, R. Kahraman, N.G. Ozerkan, N.A. Alnuaimi, B. Gencturk, M. Dawood, et al., Reinforced concrete degradation in the harsh climates of the Arabian Gulf: Field study on 30-to-50-year-old structures, J. Perform. Constr. Facil. 32 (1–12) (2018), 04018059, https://doi.org/10.1061/(asce)cf.1943-5509.0001204.
[2] M. Maslehuddin, O.S.B. Al-Amoudi Mkrmra, Concrete deterioration in the Arabian Gulf- developments in preventive techniques, in: Int. Conf. Advaces Cem. BASED Mater. Appl. to Civ. infrastructure, Lahore, December 12–14, 2007.
[3] M.N. Haque, H. Al-Khaiat, Carbonation of concrete structures in hot dry coastal regions, Cem. Concr. Compos. 19 (1997) 123–129, https://doi.org/10.1016/S0958-9465(96)00047-9.
[4] Balaji K. Trilochana, A Study of Carbonation in Concrete Structures in Marine Environment, Thesis for M Tech. Department of Civil Engineering, GITAM University, Visakhapatnam, India, 2007.
[5] ASTM C143/C143M-15a, Standard Test Method for Slump of Hydraulic-Cement Concrete, ASTM International, West Conshohocken, PA, 2013, https://doi.org/10.1520/C0143_C0143M-15A, 2015.
[6] M.G. Sohail, B. Wang, A. Jain, R. Kahraman, N.G. Ozerkan, B. Gencturk, et al., Advancements in concrete mix designs: High-performance and ultrahigh-performance concretes from 1970 to 2016, J. Mater. Civ. Eng. 30 (2018), 04017310, https://doi.org/10.1061/(ASCE)MT.1943-5533.0002144.
[7] E. Fehling, S. Michael, W. Joost, et al., Ultra-High Performance Concrete UHPC: Fundamentals, Design, Examples, 2014.
[8] K. Wille, A.E. Naaman, S. El-Tawil, G.J. Parra-Montesinos, Ultra-high performance concrete and fiber reinforced concrete: Achieving strength and ductility without heat curing, Mater. Struct. 45 (2012) 309–324, https://doi.org/10.1617/s11527-011-9767-0.
[9] B. Graybeal, J. Tanesi, Durability of an ultrahigh-performance concrete, J. Mater. Civ. Eng. 19 (2007) 848–854, https://doi.org/10.1061/(ASCE)0899-1561(2007)19:10(848).
[10] K. Wille, A.E. Naaman, S. El-Tawil, Optimizing ultra-high performance fiber-reinforced concrete, Concr. Int. 33 (2011) 35–41.
[11] R. Yu, P. Spiesz, H.J.H. Brouwers, Development of ultra-high performance fibre reinforced concrete (UHPFRC): Towards an efficient utilization of binders and fibres, Constr. Build. Mater. 79 (2015) 273–282, https://doi.org/10.1016/j.conbuildmat.2015.01.050.
[12] G.H. Russel, B a Graybeal, Ultra-High Performance Concrete : A State-Of-The-Art Report for the Bridge Community. Research, Development, and Technology Turner-Fairbank Highway Research Center 6300 Georgetown Pike McLean, A, 2013, pp. 22101–22296.
[13] K. Habel, M. Viviani, E. Denarié, E. Brühwiler, Development of the mechanical properties of an ultra-high performance fiber reinforced concrete (UHPFRC), Cem. Concr. Res. 36 (2006) 1362–1370, https://doi.org/10.1016/j.cemconres.2006.03.009.
[14] M.M. Reda, N.G. Shrive, J.E. Gillott, Microstructural investigation of innovative UHPC, Cem. Concr. Res. 29 (1999) 323–329, https://doi.org/10.1016/S0008-8846(98)00225-7.
[15] K. Wille, A.E. Naaman, G.J. Parra-Montesinos, Ultra-high performance concrete with compressive strength exceeding 150 MPa (22 ksi): A simpler way, Mater. J. 108 (2011) 46–54.
[16] R. Deeb, A. Ghanbari, B.L. Karihaloo, Development of self-compacting high and ultra high performance concretes with and without steel fibres, Cem. Concr. Compos. 34 (2012) 185–190, https://doi.org/10.1016/j.cemconcomp.2011.11.001.
[17] P.S. Rui Yu, Mix design and properties assessment of ultra-high performance fibre reinforced concrete (UHPFRC), Cem. Concr. Res. 56 (2014) 29–39, https://doi.org/10.1016/j.cemconres.2013.11.002.
[18] C. Wang, C. Yang, F. Liu, C. Wan, X. Pu, Preparation of ultra-high performance concrete with common technology and materials, Cem. Concr. Compos. 34 (2012) 538–544, https://doi.org/10.1016/j.cemconcomp.2011.11.005.
[19] R. Yu, P. Spiesz, H.J.H. Brouwers, Development of an eco-friendly Ultra-High Performance Concrete (UHPC) with efficient cement and mineral admixtures uses, Cem. Concr. Compos. 55 (2015), https://doi.org/10.1016/j.cemconcomp.2014.09.024.
[20] J.E. Funk, D.R. Dinger, Introduction to Predictive Process Control. Predict. Process Control Crowded Part. Suspens, Springer US, 1994, pp. 1–16.
[21] F. de Larrard, T. Sedran, Mixture-proportioning of high-performance concrete, Cem. Concr. Res. 32 (2002) 1699–1704, https://doi.org/10.1016/S0008-8846(02)00861-X.
[22] H.H.C. Wong, A.K.H. Kwan, Packing density of cementitious materials: Part 1—Measurement using a wet packing method, Mater. Struct. 41 (2008) 689–701, https://doi.org/10.1617/s11527-007-9274-5.
[23] A.K.H. Kwan, H.H.C. Wong, Packing density of cementitious materials: Part 2—Packing and flow of OPC + PFA + CSF, Mater. Struct. 41 (2008) 773–784, https://doi.org/10.1617/s11527-007-9281-6.
[24] P. Aghdasi, A.E. Heid, S.-H. Chao, Developing ultra-high-performance fiber-reinforced concrete for large-scale structural applications, ACI Mater. J. 113 (2016), https://doi.org/10.14359/51689103.

[25] M. Alkaysi, S. El-Tawil, Z. Liu, W. Hansen, Effects of silica powder and cement type on durability of ultra high performance concrete (UHPC), Cem. Concr. Compos. 66 (2016), https://doi.org/10.1016/j.cemconcomp.2015.11.005.
[26] TL Vande Voort, Design and Field Testing of Tapered H-Shaped Ultra High Performance Concrete Piles, 2008.
[27] C.M. Tam, V.W.Y. Tam, K.M. Ng, Assessing drying shrinkage and water permeability of reactive powder concrete produced in Hong Kong, Constr. Build. Mater. 26 (2012) 79–89, https://doi.org/10.1016/j.conbuildmat.2011.05.006.
[28] N. Roux, C. Andrade, M.A. Sanjuan, Experimental study OF durability OF reactive powder concretes, J. Mater. Civ. Eng. 8 (1996) 1–6.
[29] O. Bonneau, M. Lachemi, É. Dallaire, J. Dugat, P.C. Aïtcin, Mechanical properties and durability of two industrial reactive powder concretes, ACI Mater. J. 94 (1997) 286–290, https://doi.org/10.14359/310.
[30] P. Richard, M. Cheyrezy, Composition of reactive powder concretes, Cem. Concr. Res. 25 (1995) 1501–1511, https://doi.org/10.1016/0008-8846(95)00144-2.
[31] V. Patel, Sorptivity Testing to Assess Durability of Concrete against Freeze-Thaw Cycling, McGill University Montreal, Canada, 2009. https://escholarship.mcgill.ca/concern/theses/1g05fc626.
[32] W.P. Dias, Reduction of concrete sorptivity with age through carbonation, Cem. Concr. Res. 30 (2000) 1255–1261, https://doi.org/10.1016/S0008-8846(00)00311-2.
[33] D.Y. Yoo, W. Shin, B. Chun, N. Banthia, Assessment of steel fiber corrosion in self-healed ultra-high-performance fiber-reinforced concrete and its effect on tensile performance, Cem. Concr. Res. 133 (2020), https://doi.org/10.1016/j.cemconres.2020.106091, 106091.
[34] D.Y. Yoo, W. Shin, B. Chun, Corrosion effect on tensile behavior of ultra-high-performance concrete reinforced with straight steel fibers, Cem. Concr. Compos. 109 (2020), https://doi.org/10.1016/j.cemconcomp.2020.103566, 103566.
[35] AFGC, Ultra High Performance Fibre-Reinforced Concretes. Interim Recommendations. Association Francaise de Genie Civil (AFGC), publication, Bagneux, France, 2013.
[36] K. Hashimoto, T. Toyoda, H. Yokota, K. Kono, T. Kawaguchi, Tension-softening behavior and chloride ion diffusivity of cracked ultra high strength fiber reinforced concrete, in: RILEM-Fib-AFGC Int Symp Ultra-High Perform Fibre-Reinforced Concr UHPFRC 2013, 2013, pp. 257–264.
[37] Al Khalij, Al Cement, Cement Qatari Investors Group, Al Khalij Cem Company, Doha, Qatar, 2020 (Accessed 29 March, 2020), https://www.qatariinvestors.com/english/doing-business-with-us/products-services/cement/.
[38] P.C.485 Epsilon, New Generation Polycarboxylate Either Superplasticizer for the Precast Industry, Sodam Co/Weber Saint-Gobain, 2020.
[39] O. Bonneau, C. Vernet, M. Moranville, P.C. Aïtcin, Characterization of the granular packing and percolation threshold of reactive powder concrete, Cem. Concr. Res. 30 (2000) 1861–1867, https://doi.org/10.1016/S0008-8846(00)00300-8.
[40] ASTM C1437-15, Standard Test Method for Flow of Hydraulic Cement Mortar, ASTM International, West Conshohocken, PA, 2015, https://doi.org/10.1520/C1437-15, 2015.
[41] ACI Committee-318, Building Code Requirements for Structural Concrete (ACI 318-95) and Commentary (ACI 318R-95), American Concrete Institute, 1995.
[42] J. Dils, G. De Schutter, V. Boel, Influence of mixing procedure and mixer type on fresh and hardened properties of concrete: A review, Mater. Struct. 45 (2012) 1673–1683, https://doi.org/10.1617/s11527-012-9864-8.
[43] N.V. Tue, J. Ma, O. Marko, Influence of addition method of suplerplasticizer on the properties of fresh UHPC, in: M. Schmidt, E. Fehling, C. Glotzbach, S. Fröhlich, S. Piotrowski (Eds.), Third Int. Symp. UHPC; Kassel, Ger, Kassel University Press, Kassel Germany, 2008, pp. 93–100.
[44] B.A. Graybeal, Material Property Characterization of Ultra-high Performance Concrete, PSI, Inc. 2930 Eskridge Road Fairfax, 2006. VA 22031.
[45] ASTM C1611/C1611M-14, Standard Test Method for Slump Flow of Self-Consolidating Concrete, ASTM International, West Conshohocken, PA, 2014, https://doi.org/10.1520/C1611_C1611M-14, 2014.
[46] ASTM C39/C39M-17, Standard Test Method for Compressive Strength of Cylindrical Concrete Specimens, ASTM International, West Conshohocken, PA, 2017, https://doi.org/10.1520/C0039_C0039M-17, 2017.
[47] ASTM C78/C78M-15a, Standard Test Method for Flexural Strength of Concrete (Using Simple Beam with Third-Point Loading). West Conshohocken, PA, 2015, https://doi.org/10.1520/C0078.
[48] C. Andrade, C. Alonso, Corrosion rate monitoring in the laboratory and on-site, Constr. Build. Mater. 10 (1996) 315–328, https://doi.org/10.1016/0950-0618(95)00044-5.
[49] R. Polder, C. Andrade, B. Elsener, Ø. Vennesland, J. Gulikers, R. Weidert, et al., Test methods for on site measurement of resistivity of concrete, Mater. Struct. 33 (2000) 603–611, https://doi.org/10.1007/BF02480599.
[50] Aashto TP 95, Standard Method of Test for Surface Resistivity Indication of Concrete's Ability to Resist Chloride Ion Penetration, American Association of State Highway and Transportation Officials, Washington, DC, 2011.
[51] N. Residbegovic, A. Dzananovic, A comparative Analysis of Surface electrical resistivity in Concrete with different compositions, Technol. Sci. Int. Sci. J. Tech. Sci. (2018) 69–74.
[52] L. Hamed, G. Pouria, R. AA, S. Mustafa, Electrical resistivity of concrete - Concepts, applications, and measurement techniques, Concr. Int. 41–6 (2015).
[53] ASTM C1202-12, Standard Test Method for Electrical Indication of Concrete's Ability to Resist Chloride Ion Penetration, ASTM International, West Conshohocken, PA, 2012, https://doi.org/10.1520/C1202-12, 2012.
[54] ASTM:C1754/C1754M-12, Standard Test Method for Density and Void Content of Hardened Pervious Concrete, ASTM International, West Conshohocken, PA, 2012, https://doi.org/10.1520/C1754_C1754M-12.
[55] ASTM C 1585-13, Standard Test Method for Measurement of Rate of Absorption of Water by Hydraulic-Cement Concretes, ASTM International, West Conshohocken, PA, 2013, https://doi.org/10.1520/C1585-13, 2013.
[56] ASTM C1556-11a, Standard Determining the Apparent Chloride Diffusion Coefficient of Cementitious Mixtures by Bulk Diffusion, ASTM International, West Conshohocken, PA, 2016, https://doi.org/10.1520/C1556-11AR16, 2016.
[57] BS 1881, Part-124. British Standard Testing Concrete Part 124. Methods for Analysis of Hardened Concrete, 1998.
[58] D. Smith, The Development of a Rapid Test for Determining the Transport Properties of Concrete, University of New Brunswick, 2006.
[59] C.P. Vernet, Ultra-durable concretes: Structure at the micro- and nanoscale, MRS Bull. 29 (2004) 324–327, https://doi.org/10.1557/mrs2004.98.
[60] S. Abbas, M.L. Nehdi, M.A. Saleem, Ultra-high performance concrete: Mechanical performance, durability, sustainability and implementation challenges, Int. J. Concr. Struct. Mater. 10 (2016) 271–295, https://doi.org/10.1007/s40069-016-0157-4.
[61] J. Piérard, B. Dooms, N. Cauberg, Evaluation of durability parameters of UHPC using accelerated lab tests, in: Int. Symp. Ultra High Perform. Concr., 2012.
[62] J.P. Broomfield, Corrosion of Steel in Concrete, Understanding, Investigation and Repair, Taylor & Francis, London, 2007, https://doi.org/10.1007/s13398-014-0173-7.2.
[63] H. Yu, K.K. Chiang, L. Yang, Threshold chloride level and characteristics of reinforcement corrosion initiation in simulated concrete pore solutions, Constr. Build. Mater. 26 (2012) 723–729, https://doi.org/10.1016/j.conbuildmat.2011.06.079.